A Bioinspired Soft Actuated Material

*Ellen T. Roche, Robert Wohlfarth, Johannes T. B. Overvelde, Nikolay V. Vasilyev, Frank A. Pigula, David J. Mooney, Katia Bertoldi, and Conor J. Walsh**

Nature has abundant examples of soft muscular systems; examples of these in the human body are the stomach, tongue, diaphragm and heart. In fact, musculature has been deemed the "prototypical soft actuator" because it can achieve fast, strong actuation and remarkably complex patterns of movement.[1] Replication of these motions with traditional robotic systems is challenging, and involves complex mechanisms and many actuators. Furthermore, while the impedance of a robotic system can be modulated using force feedback and advanced control methods, it is difficult to achieve values similar to biological tissue. The emerging field of "soft robotics" lends itself to replicating biomimetic motions, having simple and low cost actuation and the capability to achieve bending, twisting, extension and flexion with non-rigid materials. However, complex motion often requires specifically designed actuators with multiple internal channels or complex cavities for actuation.[1–6] As depicted in **Figure 1**a, if we look to biology for inspiration, complex motion in soft muscular structures is often achieved through the functional arrangement of many simple contractile elements arranged spatially in a soft matrix (Figure 1b), and actuated synergistically.

In this communication we begin by realizing a soft contractile actuator that lends itself to being made from, and embedded in, an elastomeric matrix with mechanical properties similar to tissue (Figure 1c). Through the specific arrangement of the contractile elements and their selective activation, a wide variety of motions can be achieved relatively simply and inexpensively (Figure 1d). By varying matrix material, width, number of actuators and actuator spacing we characterize effects on horizontal and vertical strain distribution, and total force generation for a variety of test specimens. Furthermore, we develop methods for numerically simulating these materials that can provide design guidelines on how the material and geometric properties of both the contractile elements and matrices affect the resultant movement. To demonstrate the modeling approach and manufacturing capabilities of this new platform of materials, we present a specific case study of a material that mimics the biological form/function relationship of the left ventricle of the heart (Figure 1e). This modeling approach was verified via a prototype fabricated with a multi-step molding process that included features to aid with three dimensional measurement of movement (Figure 1f). This class of programmable, soft actuated material with multiple degrees of freedom has potential for a huge range of applications including simulating normal physiological and pathological motion, in addition to replacing or restoring the function of failing organs.

We selected McKibben pneumatic artificial muscles (PAMs)[7–9] to act as the contractile elements for this platform of materials. These are the most highly developed and studied class of soft actuators[1]. They consist of an inflatable bladder surrounded by a braided mesh. The rationale for selection of these PAMs were multiple; (i) they can be fabricated to be fully soft,[10] (ii) they can be actuated to achieve significant contraction with low pressures (demonstrating a load-length behaviour similar to muscle),[1] (ii) they can be actuated quickly (0.05 seconds dynamic response time)[10] and (iv) they can be easily integrated into the manufacture of three dimensional soft actuated materials through a multi-step co-molding process. PAMs are limited in that they can only have one mode of actuation; axial contraction with an accompanied radial expansion in response to an increase in pressure. However, if arranged spatially in a matrix according to a desired function, they may be analogous to individual contractile elements such as muscle fibrils[1] and more complex three dimensional resultant motions can be achieved. For our application, soft low-threshold pressure actuators were fabricated as described previously[10] but scaled down in size to a nominal length and diameter of 75 mm and 5 mm respectively. **Figure 2**a shows the fabrication of the actuators. A 3D printed mold (Objet Connex 500, Stratasys) was used to cast inner tubes from elastomer (Ecoflex 00–30, Smooth-on Inc.). The process is described further in the Supporting Information (Figure S1). A mesh was then placed around this inner tube and an air supply tube was secured inside actuator with nylon thread. Finally the mesh and inner tube were covered with an additional layer of elastomer. The principle of operation of the PAMs is shown in Figure 2b and Supporting Information Movie S1. Their longitudinal contraction and radial expansion

E. T. Roche, J. T.B. Overvelde, Prof. D. J. Mooney, Prof. K. Bertoldi, Prof. C. J. Walsh
School of Engineering and Applied Sciences
Harvard University
Pierce Hall, 29 Oxford Street
Cambridge, MA, 02138, USA
E-mail: walsh@seas.harvard.edu
E. T. Roche, Prof. D. J. Mooney, Prof. C. J. Walsh
Wyss Institute for Biologically Inspired Engineering
Harvard University
3 Blackfan circle, Boston, MA, 02155, USA
R. Wohlfarth
Technical University of Munich
Germany, Arcisstr. 21, D-80333, Munich, Germany
J. T. B. Overvelde, Prof. K. Bertoldi
Kavli Institute for Bionano Science and Technology
Harvard University
29 Oxford Street, Cambridge, MA, 02138, USA
Dr. N. V. Vasilyev, Dr. F. A. Pigula
Department of Cardiac Surgery
Boston Children's Hospital
300 Longwood Ave, Boston, MA, 02115, USA

DOI: 10.1002/adma.201304018

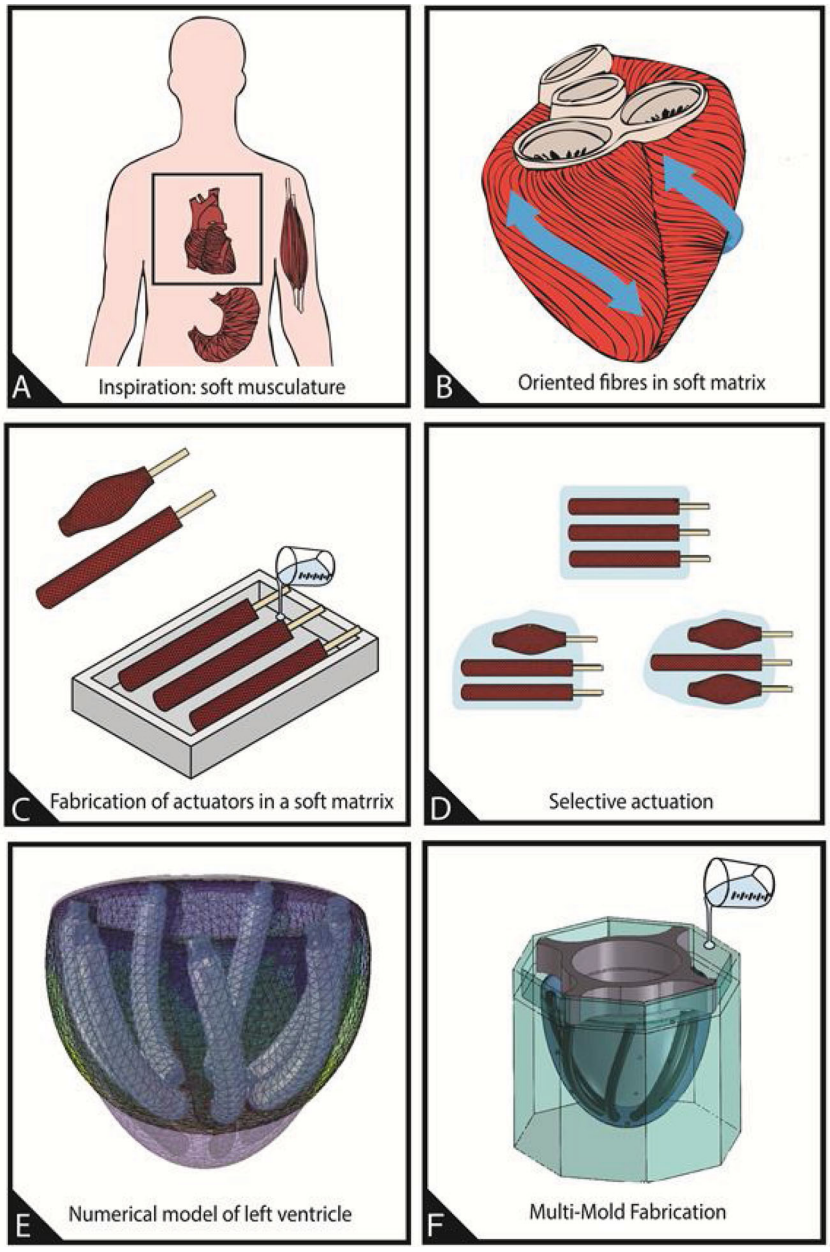

Figure 1. Inspiration, concept and realization of bioinspired soft actuated material for physiological motion generation. a) The arrangement of fibers in the heart, stomach and skeletal muscle can inspire soft actuated materials. b) Arrangement of fibers in the heart. c) Pneumatic air muscle showing displacement when actuated with air, and process of embedding actuators in a soft matrix. d) Selective activation of individual contractile elements. e) Resulting active left ventricle that can achieve twisting motion. f) Casting of actuators in a simplified bioinspired 3D structure.

were characterized, and are plotted as a function of input pressure (Figure 2c). As can be seen, the majority of the contraction/expansion occurs at low pressures due to the low durometer of the inner elastomeric tube.

In order to understand the behavior of a composite material consisting of actuators embedded in an elastomeric matrix, we manufactured a number of two dimensional test specimens with varying material properties and actuator number and spacing. Figure 2d shows the process for fabrication of dog-bone shaped test specimens with embedded actuators (one or three) with two different elastomeric matrices (Ecoflex 00–30, Smooth-on Inc. and Elastosil M4601, Wacker Chemie AG). Two-part molds were 3D printed that included interdigitating features to provide increased tensile strength at the material interface between the specimen and its ends that were clamped in the tensile testing machine. Before casting the specimens, the actuator and supply lines were placed in the mold and PDMS and Ecoflex elastomer were poured into the ends and main cavity respectively and the two materials bonded at the interdigitating interface. Optical markers were added to test specimens with a template and a Matlab (Mathworks Inc.) interface was used to track them. Strain measurements were made according to the equations in Figure 2e. Testing for force and strain at various input pressures was carried out as described in the experimental section, with more detail and results in supporting information (Supporting Information Figure S4 and S5 and Movie S2). Ecoflex 00–30 was selected as the matrix for fabrication of the soft actuated material due to the ability to generate larger strains, and because its reported modulus 125kPa[11] was within the range of reported values for myocardial tissue (230.3 ± 55.6 kPa for healthy myocardium and 117.3 ± 37.0 kPa for infarcted myocardium).[12]

Having ascertained the properties of the individual actuator and composite actuator-matrix specimens, we developed a methodology for creating numerical simulations of our soft actuated materials. The simulations were performed using the nonlinear finite element (FE) code ABAQUS/Explicit and provide a means to predict the performance of different design iterations of the soft active materials. To model the response of the actuators to an increase in pressure, without the need for a detailed model of the braided mesh, we used temperature and orthotropic coefficients of thermal expansion to model their anisotropic strain response. PAMs were assigned an experimentally derived modulus of 1.78MPa (described further in Experimental Section and Supporting Information Figure S1) and orthotropic thermal expansion coefficients according to experimentally derived strains that were negative in the longitudinal direction and positive in the radial direction for a positive change in pressure (Figure 2c). The host elastomeric matrix was modeled as an elastic material as strains were in the linear elastic range. It was assigned a thermal expansion coefficient of zero. The model of the matrix and the PAMs were

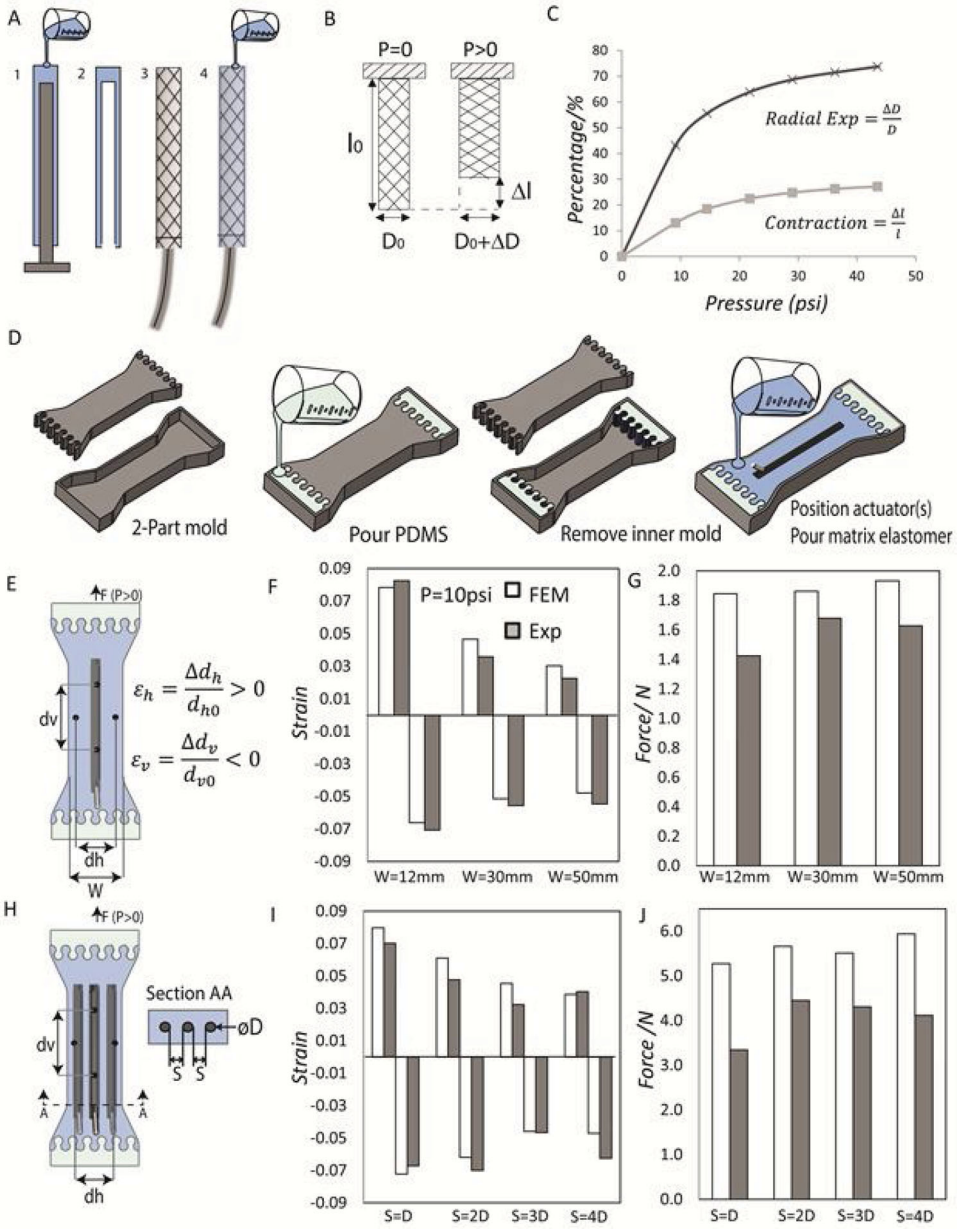

Figure 2. a) Molding process for actuators 1: An elastomeric tube is molded and capped with a 3D printed mold, and centre rod 2: Tube is demolded 3: A mesh is placed over the elastomeric tube, secured to an air supply tube, and 4: Actuator is embedded in a thin layer of elastomer. b) Operation of actuators: when pressure is applied the actuator shortens and expands radially. c) Percentage longitudinal shortening and radial expansion for each pressure. d) Fabrication process for test specimens. e) Test specimen showing optical marker placement for horizontal and vertical strain calculations and dimensions. f) Experimental and FE strain for various matrix widths. g) Experimental and FE force prediction for various matrix widths (h–j) as above for various actuator spacing (S) in terms of resting diameter of actuator, D = 5 mm.

merged in ABAQUS before applying a uniform temperature (corresponding to actuation pressure) to the entire assembly. The output for each specimen was the reaction force at fixed ends and displacement for selected nodes corresponding to the optically tracked markers on the physical specimens. In Figure 2f–j we compare numerical and experimental strain and force results for single and multiple actuators, respectively. We see very good agreement for strain; as shown in Figure 2f and 2i, with discrepancies likely due to quality and consistency of optical markers. Also, as we would expect, we observe a trend towards decreasing strain as matrix width or actuator spacing increases. The total force produced by the specimens is less affected by matrix width and actuator spacing (Figures 2g and 2j). Discrepancies between the experimental and numerically predicted force were observed (Figure 2j) with the experimental force being less than the numerical prediction. This may be attributed to some slippage of the test specimens from the grips of the tensile testing machine, or some slight de-lamination at

the actuator/matrix or matrix/PDMS interface, although measures were taken to minimize these experimental artifacts. In addition, a limitation of the numerical modeling approach is that it is not as accurate for higher pressures and higher modulus matrices.

Upon establishing the fabrication method, completing the experimental characterization, and developing and validating a numerical simulation approach, we then took inspiration from nature to create a three dimensional soft active material. The left ventricle of the heart is a muscular structure capable of achieving complex motion through oriented active contractile elements. During the contraction phase of the cardiac cycle the apex of the left ventricle twists anti-clockwise approximately 6–10° when viewed from the apex while the base of the heart has a net clockwise rotation of 2–4°.[13,14] **Figure 3**a describes the resultant complex left ventricular (LV) twisting motion, with the apex and base rotating in opposite directions. Twist is governed by parameters including orientation of the heart muscle (myocardial) fibers and the balance between the contraction of the outer (sub-epicardial) and inner (sub-endocardial) fibers which are arranged in opposing helices (Figure 3b).[15]

Once we had validated our modeling approach, we created a three-dimensional FE model that represented a simplified version of the left ventricle (LV) structure (Figure 3d and e, Supporting Information Movie S3). Specifically, an ellipsoid LV geometry was generated in Solidworks (Dassault Systemes) using dimensions in the range of a previously reported simplified model[16] (specifically; base to apex 71 mm, wall thickness 10mm, radius 42mm). As the sub-epicardial fibers dominate the motion of the LV, the simplified model includes this layer alone (Figure 3b). The PAMs were oriented in a left-handed helix to mimic the architecture of the fibers of the sub-epicardial layer and were oriented, at an inclination of –60° with respect to the basal plane as described by Young and Cowan.[17] Three transverse reference planes (apical, mid and basal) were created in the LV model (Figure 3b) and four equally spaced nodes were created on each plane coincident with the outside of the LV wall for outputting displacement data. The simulations were run as described for the 2D specimens. The boundary conditions matched that of the physical prototype when the displacement of the nodes at the base was fixed in all directions. Positional coordinates of each displacement tracking node were measured for actuation of PAMs at different pressures. Guided by this numerical simulation, a physical prototype was fabricated with identical dimensions (Figure 3c). Figure S6 describes the multi-step molding process with reconfigurable 3D printed molds that include alignment features for accurately embedding multiple actuators in an elastomeric LV structure. Motion was tracked using electromagnetic trackers (3D Guidance trakSTAR system, Ascension Technology Corporation) placed in the LV model at locations corresponding to the displacement tracking nodes in the FE model (Figure S8). Rotation of each node in the basal and apical plane for incremental pressures was calculated from these coordinates using equation 2 (Supporting Information).

The FE model predicted an apical rotation of 7.78° ± 0.55° (average of rotations for four nodes corresponding to EM trackers) when the LV is rigidly supported at the base, corresponding to the experimental boundary condition. Experimental measurements on the physical prototype closely matched that of the FE model with an agreement of 98.5%. The average experimental rotation was 7.89° ± 0.59° (Figure 3f, Movie S4 and S5). Differences between numerical and experimental results are likely due to slight discrepancies in sensor positioning in the physical prototype. Discrepancies are lower than the 2D test specimens because the electromagnetic trackers are smaller and more accurate than optical marker tracking. Both numerical and experimental values for rotation fall within the ranges of clinical values of 6.8° ± 2.5° as reported by Nagel et al.[13] Furthermore, when the physical model was supported by a flexible band rather than a rigid support to allow apical and basal rotation (end of Movie S4), apical rotation of 6.25° ± 1.73° (counterclockwise when viewed from apex) and basal rotation of 2.78°± 0.45° (clockwise) could be achieved. These values were also in the range of clinical values for apical and basal rotation respectively (6.8° ± 2.5° and 4.4° ± 1.6°) (Figure 3g). The validation of the FE model with experimental testing, and the close correlation of both with clinical data is a key result that demonstrates the applicability of this class of materials.

Left ventricular twist is a useful index of cardiac performance and myocardial mechanics, and can be affected by a range of diseases.[14] For example, if muscles are injured by ischemia (insufficient supply of blood, usually due to a blocked artery) it can lead to tissue death or infarction. This injury can render them non-contractile, leading to local akinesia (no motion) or dyskinesia (local movement that opposes that of the viable myocardium). The three-dimensional simulation and physical prototype we developed were also used to explore how damage to individual contractile elements can result in akinetic motion. This could be accomplished by selective deactivation of the PAMs, representing a transmural infarct where both sup-epicardial and sub-endocardial fibers are injured by ischemia and rendered non-contractile.[17] **Figure 4** highlights this key feature of our approach: the ability to selectively deactivate individual PAMs in both numerical simulation (Figure 4a–c, Movie S7) and our experimental model (Figure 4d, Movie S6). Pathological motion was simulated by setting isotropic thermal coefficients of selected PAMs to zero in the FE model and by disconnecting the air supply for the deactivated muscles in the physical prototype. The plot in Figure 4e shows the total rotation from each of the four markers in the apical plane (FE simulation and experimental measurements) as the PAMs are sequentially deactivated. Overall rotation decreases as PAMs are deactivated sequentially. The discrepancy between simulation and experiment is likely due to slight movement of the initial marker positions when deactivating the PAMs in the physical prototype. As the results demonstrate, the contribution to rotation from markers 1 and 2, (positioned in the region where PAMs were deactivated) decreases with each PAM deactivation. Although this trend is evident for markers 1 and 2, it is more significant for marker 2 (positioned between 2 muscles that are ultimately deactivated) than marker 1 (positioned between activated and deactivated PAMs). This is analagous to a higher reduction in rotation in an infarcted region (akinetic motion) compared to a lower reduction in rotation in a peri-infarct or border zone region (dyskinetic motion).

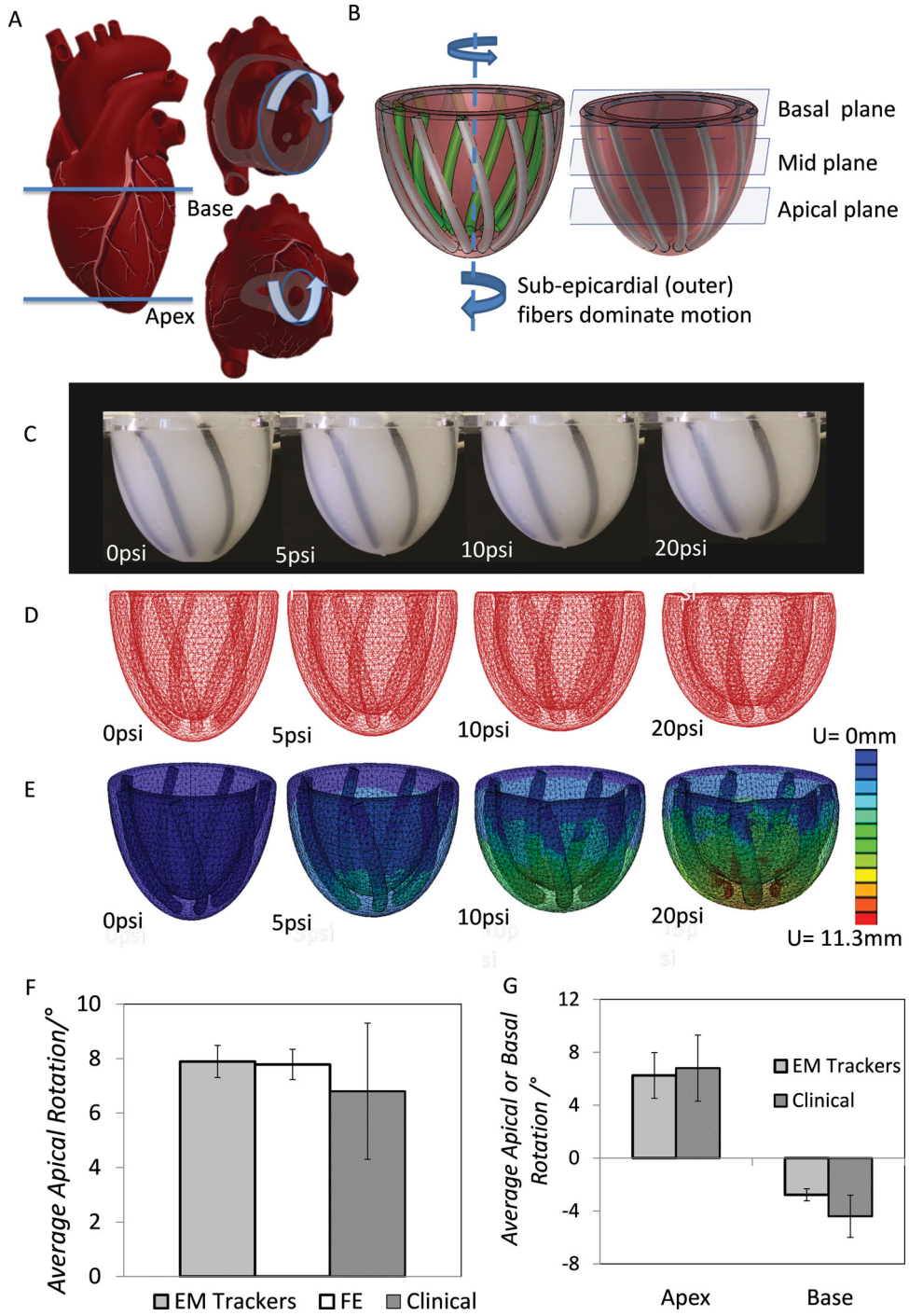

Figure 3. a) Heart with opposing rotation at apex (counter-clockwise) and base (clockwise). b) Sub-epicardial and sub-endocardial fibers are arranged in opposing helices. Sub-epicardial fibers dominate overall motion due to a larger radius, thus a greater moment arm. c) Physical prototype at various pressure increments. d) Mesh showing deformation at corresponding pressures. e) Displacement contour plot in isometric view showing the displacement (U) of the ventricle at corresponding pressures. f) Apical rotation (average of 4 markers in apical plane) for FE and physical model when LV is supported at the base compared to clinical values.[13] g) Apical and basal rotation (average of 4 markers) when LV is supported by flexible band between base and apex compared to clinical values.[13]

In this communication we have described the simulation, fabrication and experimental characterization of a soft active material concept comprising linear contractile elements completely embedded in an elastomeric matrix. A finite element based methodology was developed and validated for simulating such composite materials. A case study was presented that was inspired by the structure and dominant muscle layer of the myocardial architecture of the left ventricle. We demonstrated

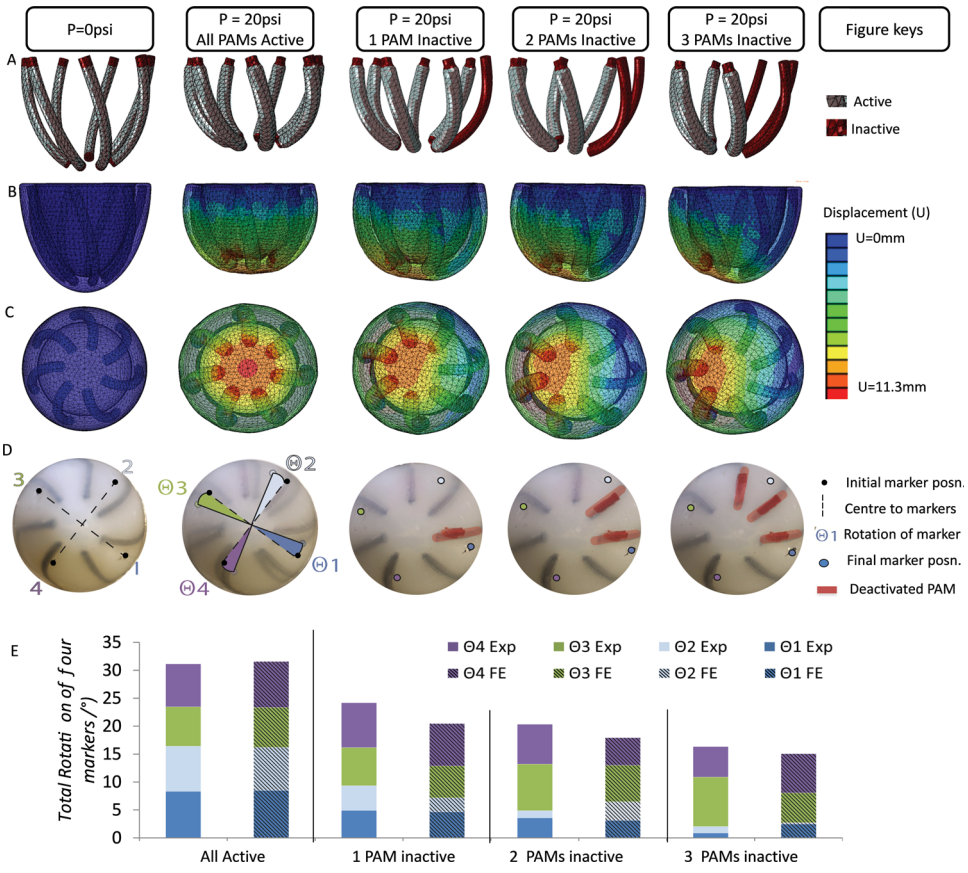

Figure 4. a) FE model showing sequential deactivation of PAMs (all at 20 psi). Displacement contour plot for each case at 20 psi viewed from anterior view (b) and apex (c), respectively. d) Physical prototype at 20 psi with 0, 1, 2, and 3 muscles deactivated (shown in red). e) Total rotation for FE model and experimental showing a decrease in rotation of markers 1 and 2 that lie in the "akinetic region".

that by mimicking the orientation of the contractile elements in a soft elastomeric material in shape similar to the left ventricle, an accurate representation of apical twist could be achieved. Furthermore, we showed that the approach could be used to predict the effect of damage to a select number of contractile elements on cardiac motion by selectively disengaging a number of PAMs. In future studies, other parameters such as changing the geometry, number and orientation of PAMS or material properties of the elastomeric matrix, could be modified to see the effect on motion. Due to the fact that physiological or pathological twist has a critical impact on the performance of implantable cardiac devices such as prosthetic valves and intracardiac defect repair devices, an ideal bench-top cardiac simulator would mimic the soft and active contractile motion of the natural heart tissue in addition to replicating physiological and pathological motions. Here, we demonstrate a soft cardiac simulator with an actively twisting component whose motion agrees well with numerical simulation and physiological clinical ranges. Given that the majority of therapy delivered to treat cardiac disease is associated with pathological motion, we also demonstrate the ability to generate pathological-like motion with our simulations and experiments by deactivating select PAMs, a key feature not present in other silicone models.[18]

Looking beyond the exemplification of the left ventricle simulator, the possible applications for this tunable platform of soft actuated materials are vast. The method of fabrication is simple, low cost and flexible. We demonstrate that by varying the matrix material, the number of actuators, actuator spacing and degree of actuation (Supporting Information, Figure S5) that we can tune the motion to match both physiological and pathological motion. In addition to increasing our understanding of these motions, this material platform can function as a test-bed for therapeutics. Additionally, as the PAMs can be further actuated, the platform could have potential as a device for the mechanical assist or replacement of organs. The elastomeric materials used in the creation of these soft active materials have a modulus on the order of 125 kPa which is closely matched to that of biological tissue, providing an inherently safer alternative for interfacing with biological tissue compared to other robotic approaches. Further tuning of the material platform could involve using an inhomogeneous or graded modulus matrix to tune the compliance of the material, or using other actuator types to achieve additional patterns of movement.

Experimental Section

Experimental Characterization of Actuators: In order to characterize longitudinal shortening and radial expansion of the actuator, one end was fixed as it was inflated to a given pressure. Length and diameter of the actuator were measured at each pressure increment. Young's

modulus of the PAMs was determined at a range of pressure increments on a mechanical tensile tester (Instron 5566, 2kN load cell) at a grip-to-grip spacing of 50mm. The crosshead was manually lowered to zero force, and then returned to the original gauge length at a speed of 200 mm/min while measuring force (Figure S2).

Experimental Characterization of Test Specimens: Specimens were gripped by rigid ends at a in a mechanical tensile tester (Instron 5566, 2kN load cell). Pressure used to actuate PAMs was varied with a regulator (Campbell Hausfeld) and measured with a sensor (Balluff BSP000W). A photo was taken at each pressure with a remote-controlled camera positioned at a fixed distance from the test specimen. Optical markers were then tracked with a camera and a customized Matlab script in order to output axial and radial strain at each pressure (Figure S4).

FE Model of Test Specimens and Left Ventricle: Quadratic tetrahedral solid hybrid elements (ABAQUS standard element type C3D10H) were used. Under large strains, Ecoflex 00–30 behaves as a hyperelastic material but strains encountered in the experiments presented are within the linear elastic range so it was modeled as a linear elastic material with properties from supplier material data sheets (density of 1.07×10^{-9} g/cm^3 and Young's modulus of 68.9kPa, the tensile strength at 100% strain) and a Poisson's ratio of 0.499. A linear elastic model was also used for the PAMs. The Young's modulus of the PAMs under tension in the axial direction was experimentally determined by measuring the force/length slope of an inflated PAM at various pressure increments (Figure S2). The composite density of the actuator was derived by the volumetric percentage of its components (elastomer, mesh, and air) and calculated at 0.45×10^{-9} g/cm^3. Air supply tube geometry and inactive ends were incorporated into the model and assigned appropriate material properties and a coefficient of thermal expansion. For the test specimens, the accuracy of the mesh was ascertained through a mesh refinement study, resulting in a mesh seeding size of 1.5 mm in the matrix and PAMs, and 4.9 mm throughout clamped ends. For the left ventricle mesh seeding size was 3.2 mm. Displacement of the nodes on the clamped ends of the samples was fixed for test specimens, and nodes at the base of the left ventricle were fixed. Orientation assignment for the PAMs in the left ventricle model is described in Supporting Information.

Experimental Characterization of Motion: Motion tracking of the physical prototype was achieved with the 3D Guidance trakSTAR (Ascension Technology Corporation) and Model 90 6DOF freedom sensors (0.9 mm). The transmitter and the base of heart were fixed in the same plane using a customized plastic holder so that the apex was free to move. One sensor was placed at the center of the base plane, and assigned as the origin. Each of eleven additional trackers were then placed at molded alignment features on the LV and then finely, symmetrically positioned with Cubes software (Ascension Technology Corporation). Insertion into the elastomer was achieved by piercing a hole with a 22 gauge needle then inserting the 0.9 mm trackers so that elastomer would self-seal around the trackers, enabling them to be secured to the elastomer. The LV was actuated in discrete pressure steps and positional data was acquired 5 times at each pressure and averaged.

Supporting Information

Supporting Information is available from Wiley Online Library or from the author.

Acknowledgements

Funding was from the Fulbright International Science and Technology Award, the Wyss Institute, and Harvard SEAS. We would like to thank Sicong Shan for initial Matlab code for optical marker tracking, Jongmin Shim and Panagiotis Polygerinos for input to FE simulation, Steven Obiajulu for help with initial actuator fabrication, the Wyss Institute for use of Object Connex 500 3D printer and Kathleen O'Donnell for help with illustrations.

Note: The value 230.3 ± 55.6 kPa given in the right-hand column of page 2 has been corrected from the incorrect value published originally.

Received: August 9, 2013
Revised: August 30, 2013
Published online: November 8, 2013

[1] F. Ilievski, A. D. Mazzeo, R. F. Shepherd, X. Chen, G. M. Whitesides, *Angew. Chem. Int. Ed.* **2011**, *50*, 1890.
[2] R. V Martinez, J. L. Branch, C. R. Fish, L. Jin, R. F. Shepherd, R. M. D. Nunes, Z. Suo, G. M. Whitesides, *Adv. Mater.* **2013**, *25*, 205.
[3] R. V. Martinez, C. R. Fish, X. Chen, G. M. Whitesides, *Adv. Funct. Mater.* **2012**, *22*, 1376.
[4] R. F. Shepherd, F. Ilievski, W. Choi, S. a. Morin, A. a. Stokes, A. D. Mazzeo, X. Chen, M. Wang, G. M. Whitesides, *Proc. Natl. Acad.Sci. USA* **2011**, 4.
[5] K. Suzumori, S. Endo, T. Kanda, *IEEE Int. Conf. Robot.* **2007**, 4975.
[6] K. Suzumori, T. Maeda, H. Watanabe, T. Hisada, *IEEE/ASME T. Mechatron.* **1997**, *2*, 281.
[7] H. A. Baldwin, in *Proceedings of the Furdt Rock Biomechanics Symposium* **1969**, 139.
[8] H. Schulte, *Natl. Acad. Sci.* **1961**, *H*, 94.
[9] M. Gavrilovic, M. R. Maric, *Med. Biol. Eng.* **1969**, *7*, 77.
[10] S. C. Obiajulu, E. T. Roche, F. A. Pigula, C. J. Walsh, in *Proc. ASME IDETC* **2013**, in press
[11] Y.-L. Park, B. Chen, D. Young, L. Stirling, R. J. Wood, E. Goldfield, R. Nagpal, *IEEE Int. Conf. Robot.* **2011**, 4488.
[12] T. Shishido, M. Sugimachi, O. Kawaguchi, H. Miyano, T. Kawada, W. Matsuura, Y. Ikeda, T. Sato, J. O. E. Alexander, K. Sunagawa, H. Miyano, T. Kawada, Y. Ikeda, T. Sato, J. Alex, *Am. J. Physiol.* **1998**, *274*, H1404.
[13] E. Nagel, M. Stuber, B. Burkhard, S. E. Fischer, M. B. Scheidegger, P. Boesiger, O. M. Hess, *Eur. Heart J.* **2000**, *21*, 582.
[14] C. H. Lorenz, J. S. Pastorek, J. M. Bundy, *J. Cardiovasc. Magn. R.* **2000**, *2*, 97.
[15] S. Nakatani, *J. Cardiovasc. Ultrasound* **2011**, *19*, 1.
[16] S. Göktepe, O. J. Abilez, K. K. Parker, E. Kuhl, *J. Theor. Biol.* **2010**, *265*, 433.
[17] A. A. Young, B. R. Cowan, *J. Cardiovasc. Magn. R.* **2012**, *14*, 49.
[18] E. R. Chamberlain, (The Chamberlain Group), *Patent US 6,685,481 B2*, **2004.**